Improvement of Power Quality Using a Robust Hybrid Series Active Power Filter

Sushree Diptimayee Swain, Pravat Kumar Ray, *Member, IEEE*, and Kanungo Barada Mohanty, *Senior Member, IEEE*

***Abstract*—The degradation in power quality causes adverse economical impact on the utilities and customers. Harmonics in current and voltage are one of the most commonly known power quality issues and are solved by the use of a hybrid series active power filter (HSAPF). In this paper, a new controller design using sliding-mode controller-2 is proposed to make the HSAPF more robust and stable. An accurate averaged model of a three-phase HSAPF is also derived in this paper. The design concept of the robust HSAPF has been verified through simulation and experimental studies, and the results obtained are discussed.**

***Index Terms*—Averaged model, hybrid active power filter, power quality, robust hybrid series active power filter (HSAPF), sliding-mode controller.**

I. Introduction

OVER the past few years, the enormous increase in the use of nonlinear loads raises many power quality issues, such as high current harmonics, voltage distortion, and low power factor, on electrical grid [1]. Hence, the proliferation of nonlinear load in the system generates harmonic currents injecting into the ac power lines. This distorted supply voltage and current causes malfunction of some protection devices, burning of transformers and motors, and overheating of cables. Hence, it is most important to install compensating devices for the compensation of harmonic currents and voltages produced due to nonlinear load. Traditionally, passive power filters (PPFs) have been used as a compensating device to compensate distortion generated by constant nonlinear loads. These filters [2] are designed to provide a low-impedance path for harmonics and maintain good power quality with a simplest design and low cost. However, passive filters have some disadvantages such as mistuning, resonance, dependence on the conditions of the power supply system, and large values of passive components that lead to bulky implementations.

For better power quality requirement, different topologies of active power filters (series active filters and shunt active filters) are connected to the nonlinear load. These filters are the most widely used solution, as they efficiently eliminate current distortion and the reactive power produced by nonlinear loads. But they are generally expensive and have high operating losses [3],[4]. Henceforth, to overcome these drawbacks and to improve the compensation performance with reduced cost of the APFs, a novel HAPF topology-III is introduced by Peng *et al.* in 1988 [5], in which the APF is connected in series with the source as well as nonlinear load, and the PPF connected in parallel with the load, which behaves as a power factor correction capacitor, is proposed. This topology [6] attracts much more attention to endure high-load currents and works as a harmonic isolator between the source and nonlinear load.

The control strategy is important to enhance the performance of a hybrid series active power filter (HSAPF). In reality, many papers for a hybrid power filter have already proposed advanced techniques to reduce current harmonics created by these nonlinear loads. In [7], a linear feedback-feed-forward controller is designed for a hybrid power filter. But this controller is not easy for getting both steady-state and transient-state performances with the linear control strategy because the dynamic model of the HSAPF system contains multiplication terms of control inputs and state variables. Due to the nonlinear characteristics of the HSAPF, a sliding-mode controller is presented in[8]. The sliding-mode control is known as an appropriate control technique for controlling nonlinear systems with uncertain dynamics and disturbances due to its order reduction property and low sensitivity to disturbances and plant parameter variations, which reduces the burden of the requirement of exact modeling. Furthermore, this sliding-mode control also diminishes the complicacy of the feedback control design by means of decoupling the system into individual subsystems of lower dimension. Because of these given properties, the implementation of the sliding-mode control can be found in the areas of power electronic switching devices. The principle of the sliding-mode control is defined as to enforce the sliding-mode motion in the predefined switching surfaces of the system state space using discontinuous control. The switching surfaces should be selected in such a way that sliding motion would maintain desired dynamics of motion according to a certain performance criterion. The conventional control methods, such as linear–quadratic regulator [9] or linear–quadratic Gaussian servo controller [10] for linear systems, are required to choose proper switching surfaces. Then, the discontinuous control needs to be chosen such that any states outside of the discontinuity surface are enforced to reach the surface at finite time. Accordingly, sliding mode occurs along the surface, and the system follows the desired system dynamics.

The main difficulty of hardware implementation of a classical sliding-mode control method is chattering. Chattering is nothing but an undesirable phenomenon of oscillation with finite

Manuscript received August 25, 2015; revised April 5, 2016 and May 23, 2016; accepted June 18, 2016. Date of publication June 30, 2016; date of current version February 2, 2017. Recommended for publication by Associate Editor K. Ngo.

The authors are with the Department of Electrical Engineering, National Institute of Technology, Rourkela 769008, India (e-mail: sushreedipti@gmail.com; rayp@nitrkl.ac.in; kbmohanty@nitrkl.ac.in).

Color versions of one or more of the figures in this paper are available online at http://ieeexplore.ieee.org.

Digital Object Identifier 10.1109/TPEL.2016.2586525

frequency and amplitude. The chattering is dangerous because the system lags control accuracy, high wear of moving mechanical parts, and high heat losses occur in electrical power circuits. Chattering occurs because of unmodeled dynamics. These unmodeled dynamics are created from servomechanisms, sensors, and data processors with smaller time constants. In the sliding-mode control, the switching frequency should be considerably high enough to make the controller more robust, stable, and no chattering because chattering reduces if switching frequency of the system increases. In the application of sliding mode controller in power converter system, the chattering problem can be reduced in the natural way by increasing switching frequency. However, it is not possible in the case of power converters because of certain limitations in switching frequency for losses in power converters, for which it results in chattering. Therefore, this chattering problem cannot blame sliding-mode implementation, since it is mainly caused by switching limitations. In [11], it is shown that the chattering exponentially tends to zero if the relative degree of the system with actuators or sensors is 2. The relative degree of the HSAPF system is 2. Because of this relative degree of the HSAPF system and also for these obstacles in a classical sliding-mode controller, this paper proposes a new controller, i.e., sliding-mode controller-2 (SMC-2). This proposed controller suppresses chattering and enhances the performance of the HSAPF. This controller is completely new for this topology of the HSAPF system. A recent research paper [12] focuses on carrier-based pulse width modulation (CBPWM) for the HSAPF topology. But, in some cases, the CBPWM-based HSAPF may not be completely measurable in most of the real-world situations. In the case of CBPWM, power system perturbations have not been taken into consideration, and also, the presence of a time delay at the reference tracking point gives rise to a slow response of the overall system. Thus, tracking error is not reduced effectively, and the stability of the system is minimally improved. To overcome this, SMC-2 is proposed for a voltage-source converter. The idea behind this controller is to achieve gain stability, perfect tracking, and distortion-free current and load voltage. In view of the above-mentioned issues, we give more emphasis on the development of the robust controller with a faster reference tracking approach in the HSAPF, which permits all perturbations such as load voltage distortion, parametric variation of load, source current distortion, and supply voltage unbalance so that compensation capability of the HSAPF system can be enhanced.

This paper is organized as follows. In Section II, the description of schematic of the system topology and hardware modules of the three-phase HSAPF model is explained. Section III depicts the averaged modeling of the HSAPF system. Section IV discloses the controller design for the HSAPF. Section V depicts the simulation as well as experimental results for harmonic compensation using the HSAPF. Section VI presents the conclusions of this paper.

II. Description of Schematic of the System Topology and Hardware Modules of the HSAPF Model

Figs. 1 and 2 demonstrate the experimental prototype and the schematic diagram of the HSAPF developed in the laboratory.

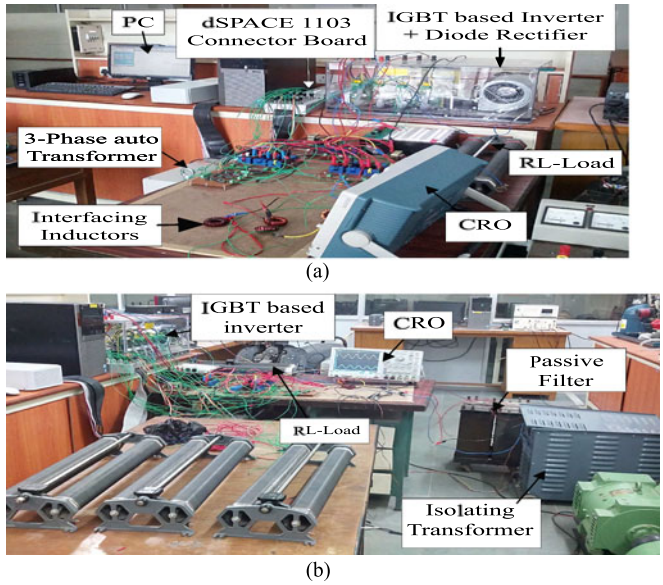

Fig. 1. (a) Experimental setup of the SAPF. (b) Experimental setup of the HSAPF.

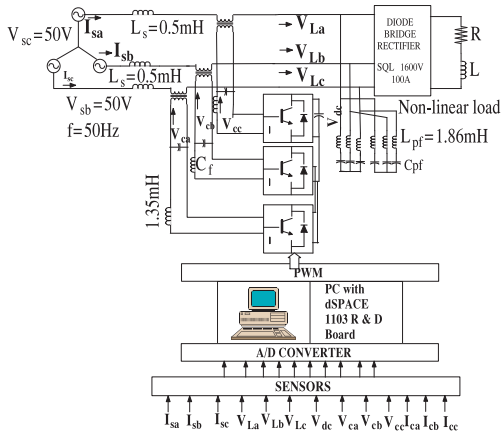

Fig. 2. Schematic diagram of the control and power circuit of the HSAPF.

This topology of the HSAPF is composed of a series-connected active power filter (SAPF) and a shunt-connected PPF. The PPF is connected in parallel with the load. The PPF consists of a fifth and seventh tuned *LC* filter of rating ($L_{pf} = 1.86$ mH and $C_{pf} = 60\,\mu$F) for the compensation of harmonic current on the load side. The SAPF is connected in series with the source through a matching transformer of a turn ratio 1:2 to ensure galvanic isolation. The SAPF consists of three parts: a three-phase insulated-gate-bipolar-transistor-based SEMIKRON inverter, a dc-link capacitor of 2200 μF, and a three-phase high-frequency *LC* filter of impedances ($C_f = 60\,\mu$F, $L_f = 1.35$ mH). The high-frequency *LC* filter is applied to get rid of high-frequency switching ripples from the compensating voltage supplied by the inverter. A nonlinear load comprising of a three-phase diode bridge rectifier (SQL 100 V, 100 A) with an *RL* load (i.e., a resistor of 8.5 A, 100 Ω, and an inductor of 40 mH) is considered. There are seven voltage sensors (LEM LV 25-P) and three current sensors (LEM LA 55-P) that are necessary. The sensors sense voltages and currents and give their input to the dSPACE 1103

TABLE I
SYSTEM PARAMETERS USED FOR SIMULATION AND EXPERIMENT

Line voltage and frequency	$V_s = 50$ V(RMS), $f = 50$ Hz
Line impedance	$L_s = 0.5$ mH, $R_s = 0.1\ \Omega$
Non-linear load impedance	$L = 40$ mH, $R = 100\ \Omega$, 8.5 A
Series active filter parameter	$C_f = 60\ \mu$F, $L_f = 1.35$ mH, $C_{dc} = 2200\ \mu$F, $V_{dc} = 40$ V
Shunt passive filter parameter	$L_{pf} = 1.86$ mH, $C_{pf} = 60\ \mu$F

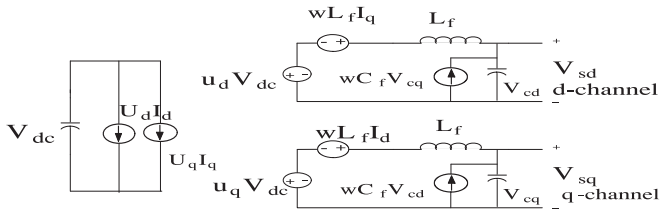

Fig. 3. Averaged equivalent circuit in a three-phase stationary frame of the HSAPF.

R and D board. The control of the HSAPF is achieved by a controller-based algorithm implemented with dSPACE 1103. First, the controller is implemented using MATLAB/Simulink. The real-time workshop is used to produce C code for real-time applications. The interface between MATLAB/Simulink and dSPACE 1103 permits running the control algorithm. The basic control structure and its mathematical equations are presented in Section IV. The switching signals are generated from the slave DSP. The generated switching pulse is used as an input to the amplifier circuit. The function of an amplifier circuit is to convert 5 to 15 V. The amplifier circuit consists of CD4504 and an isolating circuit of HCPL 2601. The output of the amplifier circuit behaved as an input to the driver of the inverter. For implementation, the control algorithm at a fixed step size of 100 μs, and hence, the maximum switching frequency of a PWM voltage-source inverter (VSI) of the HSAPF is fixed at 10 kHz. The design specifications and circuit parameters of the laboratory prototype are given in Table I.

III. AVERAGED MODELING OF THE HSAPF

Fig. 2 shows the schematic diagram of the control and power circuit of the three-phase HSAPF. The SAPF consists of a VSI connected to the grid through an *LC* filter and a three-phase linear transformer. The series resistance of the inductors is neglected. u_a, u_b, and u_c are the duty cycles of the inverter legs in a switching period, whereas V_{ca}, V_{cb}, and V_{cc} are the output voltages of the series active filter for three phases shown in Fig. 2 and I_{ca}, I_{cb}, and I_{cc} are known as the three-phase currents of the active filter; V_{aN}, V_{bN}, and V_{cN} are the phase voltages for three phases; I_{sa}, I_{sb}, and I_{sc} are known as the three-phase source currents; and V_{nN} is the neutral voltage. By averaging the inverter legs in the circuit diagram, the whole averaged model [13] of the inverter in three phases is obtained as shown in Fig. 3. From this circuit diagram, the dynamic model of the HSAPF under a synchronous reference frame can be expressed by the following differential equations:

$$\frac{di_{cd}}{dt} = \frac{V_{cd}}{L_f} + wi_{cq} - \frac{u_d V_{dc}}{L_f} \tag{1}$$

$$\frac{di_{cq}}{dt} = \frac{V_{cq}}{L_f} - wi_{cd} - \frac{u_q V_{dc}}{L_f} \tag{2}$$

$$\frac{dV_{cd}}{dt} = wV_{cq} - \frac{i_{cd}}{C_f} + \frac{i_{sd}}{C_f} \tag{3}$$

$$\frac{dV_{cq}}{dt} = -wV_{cd} - \frac{i_{cq}}{C_f} + \frac{i_{sq}}{C_f} \tag{4}$$

$$\frac{dV_{dc}}{dt} = \frac{3}{2C_{dc}}\left(u_d i_{cd} + u_q i_{cq}\right) \tag{5}$$

where V_{cd} and V_{cq} are the *dq*-axis compensating voltages, u_d and u_q are the *dq*-axis duty ratio, and ω is the angular frequency of the source voltage. To facilitate the controller design, the HSAPF system model can be defined as follows:

$$\begin{cases} x^{\cdot} = f(x) + g(x)\,u \\ y = h(x) \end{cases} \tag{6}$$

where $x = [i_{cd}, i_{cq}, V_{cd}, V_{cq}, V_{dc}]^T$ is defined as the state vector, vector $u = [u_d, u_q]^T$ stands for system control variables, and vector $y = [y_1, y_2]^T = [V_{cd}, V_{cq}]^T$ presents the system outputs. It must be noticed that the achieved multi-input multi-output system is nonlinear because of the existence of multiplication terms of the state variables and control variables. And the state variables are intensely combined with each other. These two difficulties can be accurately controlled by the design of the sliding-mode controller, which openly examine the link between the control variables and the system outputs.

IV. DEVELOPMENT OF THE CONTROL SYSTEM

A. Reference Voltage Generation Scheme (Hybrid Control Approach-Based Synchronous Reference Frame Method, HSRF)

The reference compensation voltage of the HSAPF system adopting hybrid control approach-based synchronous reference frame method is expressed as

$$V_c^* = KI_{sh} - V_{Lh}. \tag{7}$$

This hybrid control approach simultaneously detects both source current I_s as well as load voltage V_L to obtain their harmonic components. The generation of the reference compensating signal V_c^* using the combined load voltage and source current detection scheme together with an adopting hybrid control approach-based synchronous reference frame method for the HSAPF system can be obtained as (8) and (9). The realization circuit for generating V_c^* is shown in Fig. 4

$$U_d = KI_d - V_d \tag{8}$$

$$U_q = KI_q - V_q. \tag{9}$$

The generation of reference compensating signal using the combined load voltage and source current detection scheme[14] is

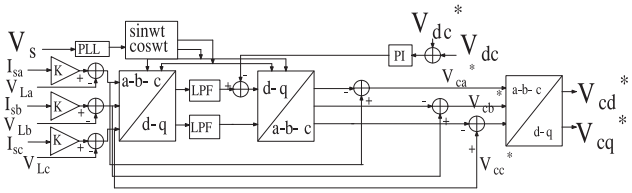

Fig. 4. Reference generation scheme (HSRF).

shown in Fig. 4. Fig. 4 shows that the error between the reference and the actual dc-link voltage of the dc-link capacitor of the three-phase PWM inverter fed from the ac system is first passed through a PI controller, and then, it is subtracted from the oscillatory component in the *d*-axis. Extra fundamental components (i.e. ΔV_{caf}, ΔV_{cbf} and ΔV_{ccf}) are added to the harmonics components in each phase. Thus, the reference compensating voltages can be expressed as

$$\left.\begin{aligned} V_{ca}^{*} &= KI_{sah} - V_{Lah} + \Delta V_{caf} \\ V_{cb}^{*} &= KI_{sbh} - V_{Lbh} + \Delta V_{cbf} \\ V_{cc}^{*} &= KI_{sch} - V_{Lch} + \Delta V_{ccf} \end{aligned}\right\}. \tag{10}$$

B. Proposed Sliding-Mode Controller Design for the HSAPF

This section describes the synthesis of the sliding-mode controller based on the averaged model of the HSAPF system. Based on the system model (6), we differentiate the compensating voltage with respect to time until the control variables u_d and u_q appear explicitly, which leads to the following equations:

$$\frac{dV_{cd}}{dt} = wV_{cq} - \frac{i_{cd}}{C_f} + \frac{i_{sd}}{C_f} \tag{11}$$

$$\frac{dV_{cq}}{dt} = -wV_{cd} - \frac{i_{cq}}{C_f} + \frac{i_{sq}}{C_f} \tag{12}$$

$$\begin{aligned} \frac{d^2V_{cd}}{dt^2} =& -w^2V_{cd} - w\frac{i_{cq}}{C_f} + w\frac{i_{sq}}{C_f} - \frac{V_{cd}}{L_fC_f} \\ & - w\frac{i_{cq}}{C_f} - \frac{u_dV_{dc}}{L_fC_f} + \frac{di_{sd}}{dt}\cdot\frac{1}{C_f} \end{aligned} \tag{13}$$

$$\begin{aligned} \frac{d^2V_{cq}}{dt^2} =& -w^2V_{cq} - w\frac{i_{cd}}{C_f} + w\frac{i_{sd}}{C_f} - \frac{V_{cq}}{L_fC_f} \\ & - w\frac{i_{cd}}{C_f} - \frac{u_qV_{dc}}{L_fC_f} + \frac{di_{sq}}{dt}\cdot\frac{1}{C_f}. \end{aligned} \tag{14}$$

So, the relative degree of the system is "2" because at the second derivative of compensating voltage in the *dq*-axis, we obtain control variables u_d and u_q. The Jacobi matrix of $j(d)$ with respect to the control vector "u" can be calculated as follows:

$$\frac{\partial j(d)}{\partial d^T} = \begin{bmatrix} \dfrac{-V_{dc}}{L_f} & 0 \\ 0 & \dfrac{-V_{dc}}{L_f} \end{bmatrix}. \tag{15}$$

In fact, the dc-link voltage V_{dc} is positive in the operating range. $\frac{\partial j(d)}{\partial d^T}$ is nonsingular. Henceforth, the relative degree vector of the system is $\beta = [\beta_1, \beta_2]^T = [2, 2]^T$, and $\beta_1 + \beta_2 = 2 + 2 = 4$ is strictly less than the system order $n = 5$. To synthesize a robust HSAPF system, a sliding-mode controller is designed based on the linearized model (6). The control objective of the HSAPF system is to force the compensating voltages V_{cd} and V_{cq}; the mathematical expressions of sliding surface are as follows:

$$\overline{S} = \begin{bmatrix} \overline{S}_d \\ \overline{S}_q \end{bmatrix} \tag{16}$$

$$\overline{S} = S + \alpha\dot{S} \tag{17}$$

$$\overline{S}_d = S_d + \dot{S}_d \tag{18}$$

$$\overline{S}_q = S_q + \dot{S}_q \tag{19}$$

putting the values of V_{cd} and V_{cq} into (20) and (22)

$$\overline{S}_d = (V_{cd} - V_{cd}^{*}) + \alpha_1\left(\dot{V}_{cd} - \dot{V_{cd}}^{*}\right) \tag{20}$$

$$\dot{\overline{S}}_d = \left(\dot{V}_{cd} - \dot{V_{cd}}^{*}\right) + \alpha_1\left(\ddot{V}_{cd} - \ddot{V_{cd}}^{*}\right) \tag{21}$$

$$\overline{S}_q = (V_{cq} - V_{cq}^{*}) + \alpha_2\left(\dot{V}_{cq} - \dot{V_{cq}}^{*}\right) \tag{22}$$

$$\dot{\overline{S}}_q = \left(\dot{V}_{cq} - \dot{V_{cq}}^{*}\right) + \alpha_2\left(\dot{V}_{cq} - \dot{V_{cq}}^{*}\right) \tag{23}$$

where α is a positive constant. The design procedure of the sliding-mode controller is depicted as

$$\dot{\overline{S}} = 0 \tag{24}$$

$$\dot{\overline{S}}_d = 0. \tag{25}$$

Substituting (11) and (13) into (25), the equivalent control law in the *d*-axis can be directly derived as

$$\begin{aligned} U_{deqv.} =& -\left(\dot{V}_{cd}^{*} + \alpha\ddot{V}_{cd}^{*}\right) + \frac{L_f}{V_{dc}}\left(C_fwV_{cq} - i_{cd} + i_{sd}\right) \\ & + \frac{\alpha L_f}{V_{dc}}\left(-C_fw^2V_{cd} - wi_{cq} + wi_{sq} - \frac{V_{cd}}{L_f} - wi_{cq} + \dot{i_{sd}}\right). \end{aligned} \tag{26}$$

Similarly, the equivalent control law in the *q*-axis can be derived as follows:

$$\begin{aligned} U_{qeqv.} =& -\left(\dot{V}_{cq}^{*} + \alpha\ddot{V}_{cq}^{*}\right) + \frac{L_f}{V_{dc}}\left(C_fwV_{cd} - i_{cq} + i_{sq}\right) \\ & + \frac{\alpha L_f}{V_{dc}}\left(-C_fw^2V_{cq} - wi_{cd} + wi_{sd} - \frac{V_{cq}}{L_f} - wi_{cd} + \dot{i_{sq}}\right) \end{aligned} \tag{27}$$

$$U = U_{eqv.} + U_{\text{switching}} \tag{28}$$

$$U_d = U_{deqv.} + U_{d\text{switching}} \tag{29}$$

$$U_q = U_{qeqv.} + U_{q\text{switching}}. \tag{30}$$

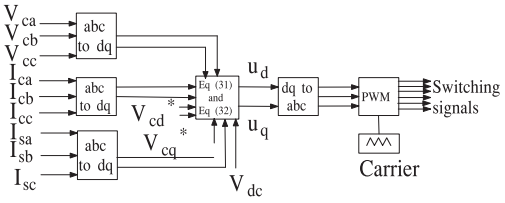

Fig. 5. Proposed sliding-mode control structure for the HSAPF.

The nonlinear control law has been directly derived by putting the values of $U_{deqv.}$ and $U_{qeqv.}$ in (29) and (30), respectively

$$U_d = -\left(\dot{V}^*_{cd} + \alpha \ddot{V}^*_{cd}\right) + \frac{L_f}{V_{dc}}\left(C_f w V_{cq} - i_{cd} + i_{sd}\right) + \frac{\alpha L_f}{V_{dc}}\left(-C_f w^2 V_{cd} - w i_{cq} + w i_{sq} - \frac{V_{cd}}{L_f} - w i_{cq} + \dot{i}_{sd}\right) - K_{11}\text{sign}\left(S_d\right) - K_{12}\text{sign}\left(\dot{S}_d\right) \quad (31)$$

$$U_q = -\left(\dot{V}^*_{cq} + \alpha \ddot{V}^*_{cq}\right) + \frac{L_f}{V_{dc}}\left(C_f w V_{cd} - i_{cq} + i_{sq}\right) + \frac{\alpha L_f}{V_{dc}}\left(-C_f w^2 V_{cq} - w i_{cd} + w i_{sd} - \frac{V_{cq}}{L_f} - w i_{cd} + \dot{i}_{sq}\right) - K_{21}\text{sign}\left(S_q\right) - K_{22}\text{sign}\left(\dot{S}_q\right). \quad (32)$$

The control block diagram of the proposed control strategy has been illustrated in Fig. 5.

The control function of this controller is as follows: $U_{\text{eq}} = U_{\text{switching}}$

$$U_{\text{eq}} = \begin{cases} +1, & \text{when } S > 0 \\ -1, & \text{when } S < 0. \end{cases} \quad (33)$$

For the satisfactory operation of the HSAPF system, this controller fulfills the stability condition.

C. Stability Analysis of the Sliding-Mode-Controller-Based HSAPF

This section analyzes the stability of the HSAPF system with the suggested control strategy. For the stability analysis of the system external dynamics of V_{cd} and V_{cq}, we define a sliding manifold as follows:

$$\overline{S} = \left[\overline{S}_d \ \overline{S}_q\right]^T = 0. \quad (34)$$

For evidence of the system stability with the sliding-mode controller, we adopt the Lyapunov function as a candidate function, i.e.,

$$V(x) = \frac{1}{2}\overline{S}^T\overline{S} \quad (35)$$

whose time derivative is

$$\dot{V} = \left[\overline{S}_d \ \overline{S}_q\right]\begin{bmatrix}\dot{\overline{S}}_d \\ \dot{\overline{S}}_q\end{bmatrix}. \quad (36)$$

Substituting (20)–(23) into (36), we can obtain

$$\dot{V} = -S_d\left(\frac{i_{cd}}{C_f} - \frac{i_{sd}}{C_f} - wV_{cq} + \dot{V}^*_{cd}\right) - S_d\alpha_1\left(-K_{11}\text{sign}\left(S_d\right) - K_{12}\text{sign}\left(\dot{S}_d\right) - \dot{V}^*_{cd}\right) - S_q\left(\frac{i_{cq}}{C_f} - \frac{i_{sq}}{C_f} - wV_{cd} + \dot{V}^*_{cd}\right) - S_q\alpha_2\left(-K_{21}\text{sign}\left(S_q\right) - K_{12}\text{sign}\left(\dot{S}_q\right) - \dot{V}^*_{cq}\right). \quad (37)$$

We can see from (37) that $\dot{V}(x) \leqslant 0$. If, in a region, there exists a scalar function $V(x)$ with continuous first partial derivatives such that $V(x)$ is positive definite and $\dot{V}(x)$ is negative semidefinite, then the equilibrium point is stable. If, actually, the derivative $\dot{V}(x)$ is locally negative definite in the existing region, then the system is stable, which means that the attractiveness of the manifold (34) is stable for the proposed SMC-2-based HSAPF.

In this proposed control approach, the control signal satisfies all the above conditions, so that the state trajectories are moved toward the switching surface. Henceforth, during the operation of this proposed controller, the HSAPF system achieves fast response, good robustness, and throwaway disturbances effectively.

V. Results and Discussions

A. Simulation Results

The reference generation approach (the HSRF method) with the switching pattern generation scheme (i.e., SMC-2) of the HSAPF system given in Fig. 2 is tested using MATLAB/Simulink software. A three-phase source voltage is applied to a harmonic voltage producing nonlinear load. This voltage producing nonlinear load comprises of a three-phase diode bridge rectifier feeding an *RL* load. Due to this type of nonlinear load, a harmonic distortion occurs in both source current and load voltage. This harmonic contamination is the reason of power quality disturbances. So, power quality disturbances can be eradicated by means of the HSAPF. The simulation and experimental parameters are encapsulated in Table I. One reference generation technique and one modulation technique, i.e., hybrid control approach-based SRF method (HSRF) and sliding-mode-controller-based HSAPF, are verified and analyzed using the following MATLAB simulation results. In order to verify the reliability of the proposed controller, the system is simulated under MATLAB/Simulink version 2010. The goal of simulation is to reduce the total harmonic distortion (THD) response of the sliding-mode-controller-based HSAPF below 5%. And an HSRF combined with the sliding-mode controller technique utilizes dc-link voltage properly for equivalent control law generation. MATLAB simulation results for source voltage V_s, load current I_L, source current I_s, dc voltage V_{dc} for steady state, and the dynamic condition of load under the existing method have been presented in Fig. 6. The nature of the source current without a filter is exactly like load current.

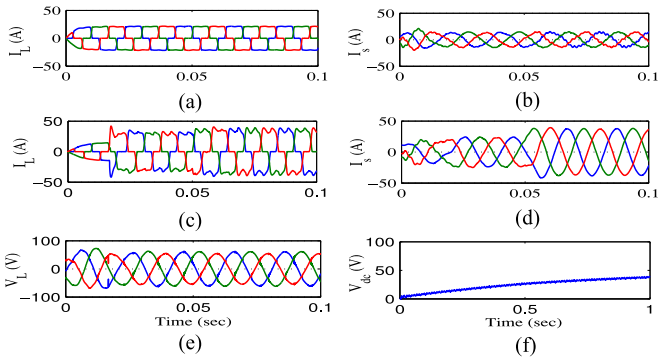

Fig. 6. (a) Steady-state response of the load current before compensation. (b) Steady-state response of the source current after compensation. (c) Transient response of the load current before compensation. (d) Transient response of the source current after compensation. (e) Load voltage after compensation. (f) DC-link voltage for the existing method (ideal sliding-mode controller).

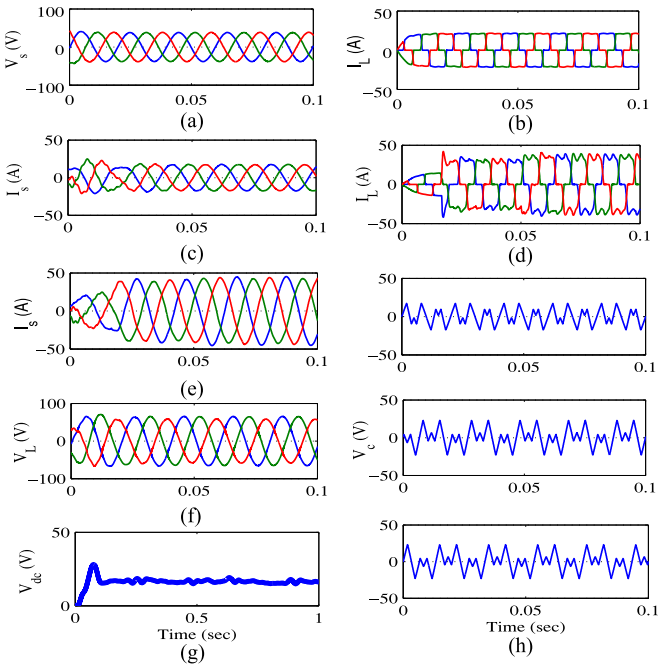

Fig. 7. (a) Source voltage. (b) Steady-state response of the load current before compensation. (c) Steady-state response of the source current after compensation. (d) Transient response of the load current before compensation. (e) Transient response of the source current after compensation. (f) Load voltage after compensation. (g) DC-link voltage. (h) Three-phase compensating voltage for the proposed controller-based HSAPF system.

MATLAB simulation results for source voltage V_s, load current I_L, source current I_s, dc voltage V_{dc} for steady state, dynamic condition of load, and parametric variation of the HSAPF system under SMC-2 have been depicted in Figs. 7 and 8. From the simulation results, it is proved that the THD response of the sliding-mode-controller-based HSAPF is smaller than the THD response of the existing technique-based HSAPF. Simulation results under several system operating conditions of load have verified the design concept of the suggested highly effective and robust sliding-mode-based HSAPF. The robustness of the proposed HSAPF has been analyzed here. In the proposed

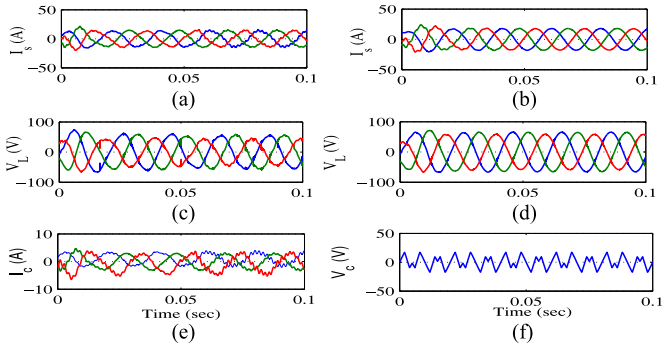

Fig. 8. (a) Three-phase source current after compensation for the existing controller-based HSAPF. (b) Three-phase source current after compensation for the proposed controller-based HSAPF. (c) Three-phase load voltage after compensation for the existing controller-based HSAPF. (d) Three-phase load voltage after compensation for the proposed controller-based HSAPF. (e) Three-phase compensating current. (f) Compensating voltage for phase-a in the parametric variation case of the HSAPF system.

controller, the source current THD is reduced from 20.14% to 1.62%. For the transient condition of load, the THD of source current for the proposed controller-based HSAPF is reduced from 26.7% to 2.16%. The harmonic compensation ratio (HCR) for steady state and the parametric variation of the HSAPF system case are approximately the same, but the HCR in the transient case of the nonlinear load is differed by only 0.55% from the above two cases. Thus, the THDs of the source current are unaffected by the parametric variations of load. This proves the robustness of the proposed HSAPF under parametric variations of load. The HCR factor is calculated as follows:

$$\text{HCR} = \frac{\text{THD}\,(\%)\ \text{After Compensation}}{\text{THD}\,(\%)\ \text{Before Compensation}} * 100\%.$$

B. Experimental Results

The proposed control algorithm has been implemented in real time on the hardware setup developed in our laboratory. A prototype of the experimental setup is shown in Fig. 1. The efficacy of the proposed scheme is compared with the existing method [15] (harmonic series compensators in power systems: their control via sliding mode), in which instantaneous reactive power theory used as a reference generation process and an ideal sliding-mode controller with carrier-based PWM is applied for switching pattern generation. The disadvantage of this controller is switching frequency, i.e., it requires high switching frequency to make the system more robust and stable, but it produces more switching loss, chattering, and white Gaussian noise. But in the case of the proposed approach, SMC-2 is employed as a voltage controller, i.e., for switching pattern generation and the HSRF method for reference voltage generation in the HSAPF. The experimental studies for both steady-state and dynamic conditions are performed and discussed in the following sections.

1) Case 1: Balanced Supply Voltages With Steady-State Load Condition: The performance of the proposed HSAPF is verified through load impedance in the initial case. A diode bridge

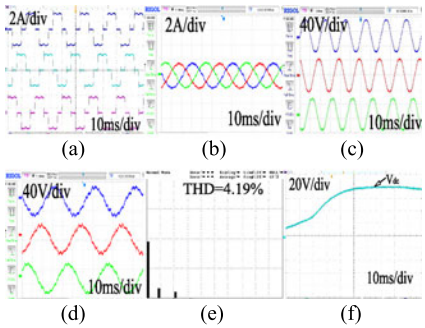

Fig. 9. *Case 1a:* (a) Three-phase load current before compensation. (b) Three-phase source current after compensation. (c) Three-phase load voltage before compensation. (d) Three-phase load voltage after compensation. (e) THD of the source current after compensation. (f) DC-link voltage in the existing method.

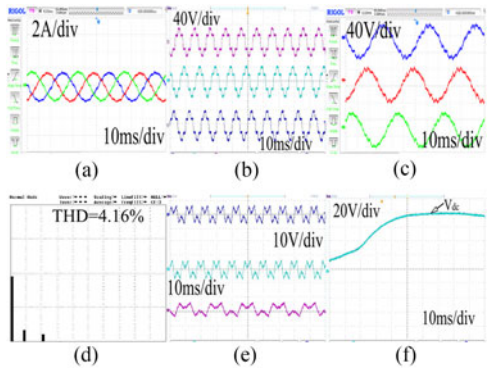

Fig. 11. *Case 2a:* (a) Three-phase source current after compensation. (b) Load voltage before compensation. (c) Load voltage after compensation. (d) THD of the source current after compensation. (e) Three-phase compensating voltage. (f) DC-link voltage in the exist method (ideal sliding-mode controller).

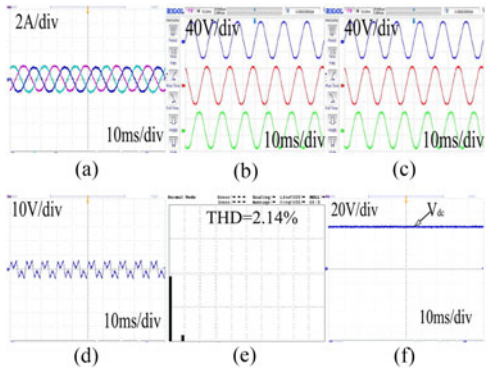

Fig. 10. *Case 1b:* (a) Three-phase source current after compensation. (b) Three-phase load voltage before compensation. (c) Three-phase load voltage after compensation. (d) Compensating voltage for phase-a. (e) THD of the source current after compensation. (f) DC-link voltage in the proposed method.

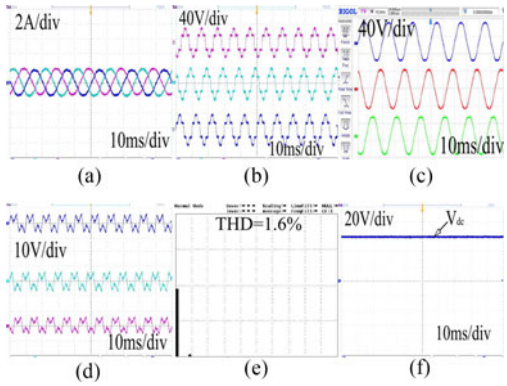

Fig. 12. *Case 2b:* (a) Three-phase source current after compensation. (b) Three-phase load voltage before compensation. (c) Three-phase load voltage after compensation. (d) Three-phase compensating voltage. (e) THD of the source current after compensation. (f) DC-link voltage for the proposed method.

rectifier with an *RL* load is selected as the test load to measure the operation of the HSAPF for load compensation. The three-phase load currents (I_{La}, I_{Lb}, I_{Lc}) before compensation are shown in Fig. 9(a). The source current is found to be sinusoidal. The source current, the load voltage, and the reference tracking behavior of the compensating voltage for both the existing and proposed methods have been presented in Figs. 9 and 10, respectively.

2) Case 2: Balanced Supply Voltages With Steady-State Load Condition as Well as Changing HSAPF Parameters: In this case, the HSAPF parameters are changed from $C_f = 50\,\mu$F, $L_f = 0.35$ mH to $C_f = 60\,\mu$F, $L_f = 1.35$ mH. Under this condition, the performance of the proposed controller has been verified with the existing method through Figs. 11 and 12. It is seen that in the case of the proposed approach, the source current are smooth and distortion is less as compared to the existing method. Hence, the effective harmonic compensation is more in the case of the proposed method. Also, the THD response of the source current after compensation is superior in the case of the proposed method over the existing method.

3) CASE 3: Balanced Supply Voltages With Dynamic Load Condition: The performance of the proposed HSAPF, assuming the balanced supply voltages, during a sudden load varying condition is illustrated in Figs. 13 and 14. To create dynamic condition, the load is changed from ($R = 100\ \Omega$, $L = 40$ mH) to ($R = 20\ \Omega$, $L = 10$ mH). When the load changes, the compensating voltage quickly responds to changes to compensate the harmonic voltage and current in the load, as shown in Fig. 13. Also, the compensated source current can be viewed from Figs. 13(a) and 14(b) for both existing and proposed methods. As noticed, the HSAPF system with the proposed approach achieves better performances in comparison to existing one. Furthermore, the dc-link voltage in the case of existing method settles to the reference value with a time delay of 0.1 s, while a delay of only 0.024 s is possible for the proposed technique, as illustrated in Figs. 13(d) and 14(c). Figs. 13 and 14 shows that the source current THD is effectively reduced from 25.9% to 2.16% and 3.25% in the proposed and existing methods, respectively. Therefore, this transient event demonstrates the actual capability and enhances the performance of the proposed approach over the existing approach.

4) Case 4: Unbalanced Supply Voltages With Steady-State Load Condition: In the previous cases, the supply voltage has been considered as sinusoidal and balanced, but this voltage

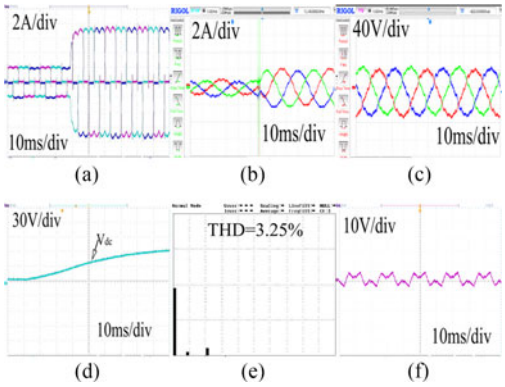

Fig. 13. *Case 3a:* (a) Three-phase load current before compensation. (b) Three-phase source current after compensation. (c) Three-phase load voltage after compensation. (d) DC-link voltage. (e) THD of the source current after compensation. (f) Compensating voltage for phase-a.

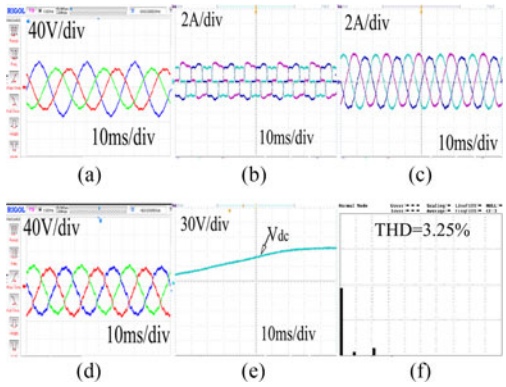

Fig. 15. *Case 4a:* (a) Three-phase source voltage before compensation. (b) Three-phase load current before compensation. (c) Three-phase source current after compensation. (d) Three-phase load voltage after compensation. (e) DC-link voltage. (f) THD of the source current after compensation.

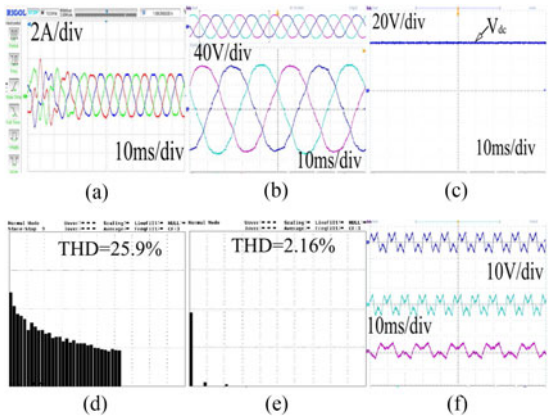

Fig. 14. *Case 3b:* (a) Three-phase source current after compensation. (b) Three-phase load voltage after compensation. (c) DC-link voltage. (d) THD of the source current before compensation. (e) THD of the source current after compensation. (f) Three-phase compensating voltage after compensation in the proposed method.

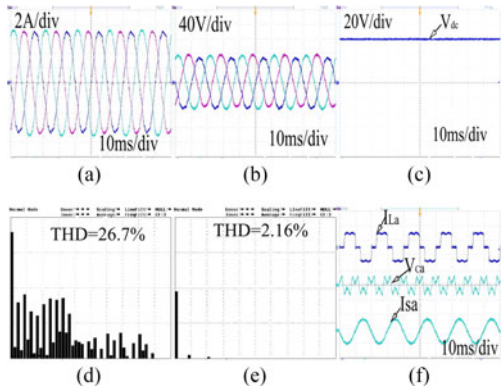

Fig. 16. *Case 4b:* (a) Three-phase source current after compensation. (b) Three-phase load voltage after compensation. (c) DC-link voltage. (d) THD of the source current before compensation. (e) THD of the source current after compensation. (f) Compensating voltage with the load current and the source current after compensation in the proposed method.

is considered as unbalanced in nature. To verify the effectiveness of the proposed control algorithm under such a condition, experiments have been carried out. The profiles for three-phase supply voltages and source currents are shown in Figs. 15 and 16, respectively. Fig. 16 shows that the harmonic compensation performance of the HSAPF has not been deteriorated at the unbalanced source voltage condition and the source currents are also balanced. But, a small number of flickers are observed in the case of the existing method. THD analysis for phase-a supply current is shown in Figs. 15 and 16; the proposed method has lower THD (i.e., 2.16%) as compared to the existing method (i.e., 3.25%), whereas the load current is distorted with a THD factor of 26.7%.

It is verified through experiments that the proposed controller-based HSAPF has better steady-state performances as well as better dynamic responses as compared to the existing approach. In addition, to evaluate the robustness performance of the existing controller and the proposed controller assuming previously mentioned four cases, HCR factors are calculated and summarized in Table II. The results of Table II demonstrate that in the case of the proposed approach, HCR factors are maintained nearly the same, i.e., 8%, and these factors are unaffected by any perturbations raised in load or source sides, such robustness cannot be achieved by using the existing control strategy, in which the HCR factor has been largely deviated in the presence

TABLE II
HARMONICS COMPENSATION EFFECT OF THE PROPOSED AND EXISTING CONTROL STRATEGY IN THE HSAPF (EXPERIMENTAL)

Cases	THD % phase-a source current			HCR (%)
	Methods used in HSAPF	Before comp. THD (%)	After comp. THD (%)	
Case 1	Proposed method	24.5	2.14	8.73
	Existing method	24.5	4.19	17.1
Case 2	Proposed method	20.14	1.6	7.94
	Existing method	20.14	4.16	20.65
Case 3	Proposed method	25.9	2.16	8.33
	Existing method	25.9	3.25	12.54
Case 4	Proposed method	26.7	2.16	8.08
	Existing method	26.7	3.25	12.17

of steady-state and parametric variation behavior of the load. Thus, the superiority of the proposed algorithm over the existing method has been highlighted through all situations of power system perturbations.

VI. Conclusion

In this paper, a new robust controller design for the HSAPF has been presented. The control design is established by SMC-2 that derives the equivalent control law. This control law is very much helpful for switching pattern generation. The robustness of the proposed controller has been verified by analyzing the performance under steady-state and transient conditions of the power system. With the application of this technique, the functionalities of the HSAPF are enhanced. From the obtained simulations as well as experimental results, the proposed HSAPF has been observed to provide efficient current as well as voltage harmonic mitigation, reference voltage tracking behavior, and reactive power compensation with dynamically varying load conditions. In the presence of an additive white noise, switching losses and distortion in both the source current and the load voltage, the SRF method is found to be the best one for reference generation. Furthermore, the main feature of SMC-2 is the variable structure control method, which reduces tracking error distortion, suppress chattering, and noise, and hence, a perfect gain stability of the HSAPF system has been achieved. The proposed filter can compensate source currents and also adjust itself to compensate for variations in nonlinear load currents, maintain dc-link voltage at steady state, and help in the correction of the power factor of the supply side adjacent to unity. Simulation and experimental results under several system-operating conditions of load have verified the design concept of the suggested sliding-mode-based HSAPF to be highly effective and robust.

References

[1] Z. Zeng, H. Yang, S. Tang, and R. Zhao, "Objective-oriented power quality compensation of multifunctional grid-tied inverters and its application in microgrids," *IEEE Trans. Power Electron.*, vol. 30, no. 3, pp. 1255–1265, Mar. 2015.

[2] A. B. Nassif, W. Xu, and W. Freitas, "An investigation on the selection of filter topologies for passive filter applications," *IEEE Trans. Power Del.*, vol. 24, no. 3, pp. 1710–1718, Jul. 2009.

[3] M. Ali, E. Laboure, and F. Costa, "Integrated active filter for differential-mode noise suppression," *IEEE Trans. Power Electron.*, vol. 29, no. 3, pp. 1053–1057, Mar. 2014.

[4] E. R. Ribeiro and I. Barbi, "Harmonic voltage reduction using a series active filter under different load conditions," *IEEE Trans. Power Electron.*, vol. 21, no. 5, pp. 1394–1402, Sep. 2006.

[5] F. Z. Peng, H. Akagi, and A. Nabae, "A new approach to harmonic compensation in power systems-a combined system of shunt passive and series active filters," *IEEE Trans. Ind. Appl.*, vol. 26, no. 6, pp. 983–990, Nov./Dec. 1990.

[6] S. Diptimayee Swain, P. K. Ray, and K. Mohanty, "Voltage compensation and stability analysis of hybrid series active filter for harmonic components," in *Proc. Annu. IEEE India Conf.*, 2013, pp. 1–6.

[7] W. Tangtheerajaroonwong, T. Hatada, K. Wada, and H. Akagi, "Design and performance of a transformerless shunt hybrid filter integrated into a three-phase diode rectifier," *IEEE Trans. Power Electron.*, vol. 22, no. 5, pp. 1882–1889, Sep. 2007.

[8] W. Guo, J. Wu, and D. Xu, "A novel sliding mode control of a high-voltage transformerless hybrid shunt active power filter," in *Proc. 4th IEEE Conf. Ind. Electron. Appl.*, 2009, pp. 2908–2913.

[9] B. Kedjar and K. Al-Haddad, "DSP-based implementation of an LQR with integral action for a three-phase three-wire shunt active power filter," *IEEE Trans. Ind. Electron.*, vol. 56, no. 8, pp. 2821–2828, Aug. 2009.

[10] R. Panigrahi, B. Subudhi, and P. C. Panda, "A robust LQG servo control strategy of shunt-active power filter for power quality enhancement," *IEEE Trans. Power Electron.*, vol. 31, no. 4, pp. 2860–2869, Apr. 2016.

[11] L. M. Fridman, "Singularly perturbed analysis of chattering in relay control systems," *IEEE Trans. Autom. Control*, vol. 47, no. 12, pp. 2079–2084, Dec. 2002.

[12] M. A. Mulla, R. Chudamani, and A. Chowdhury, "A novel control method for series hybrid active power filter working under unbalanced supply conditions," *Int. J. Elect. Power Energy Syst.*, vol. 64, pp. 328–339, 2015.

[13] S. Rahmani, K. Al-Haddad, and H. Y. Kanaan, "Average modeling and hybrid control of a three-phase series hybrid power filter," in *Proc. IEEE Int. Symp. Ind. Electron.*, 2006, vol. 2, pp. 919–924.

[14] S. D. Swain and P. K. Ray, "Harmonic current and voltage compensation using HSAPF based on hybrid control approach for synchronous reference frame method," *Int. J. Elect. Power Energy Syst.*, vol. 75, pp. 83–90, 2016.

[15] H. De Battista and R. J. Mantz, "Harmonic series compensators in power systems: Their control via sliding mode," *IEEE Trans. Control Syst. Technol.*, vol. 8, no. 6, pp. 939–947, Nov. 2000.

Sushree Diptimayee Swain is working toward the Ph.D. degree in the Department of Electrical Engineering, National Institute of Technology, Rourkela, India.

Her research interests include application of nonlinear control in power electronics.

Pravat Kumar Ray (M'13) received the Ph.D. degree in electrical engineering from the National Institute of Technology (NIT), Rourkela, India, in 2011.

He is currently an Assistant Professor with the Department of Electrical Engineering, NIT Rourkela. His research interests include power system, power quality, solar irradiance forecasting using sky images, and grid integration of renewable energy systems.

Kanungo Barada Mohanty (SM'11) received the B.Tech. degree in electrical engineering from Veer Surendra Sai University of Technology, Burla, India, in 1989, and the M.Tech. and Ph.D. degrees from Indian Institute of Technology, Kharagpur, India, in 1990 and 2002, respectively.

He has been a Faculty Member of the National Institute of Technology, Rourkela, India, since 1991, where he is an Associate Professor. His research interests include vector control and direct torque control of induction machines, wind and solar energy systems, and microgrids.

Dr. Mohanty is a Fellow of the Institution of Engineers (India) and the Institution of Electronics and Telecommunication Engineers (India).